Nanosilver Inkjet Printed CPW-Fed Flexible Antenna Sensor for Contactless Liquid Acetone/Water Detection

Kabir Hossain, *Graduate Student Member, IEEE*, Yu Dang, *Graduate Student Member, IEEE*, and Michael Cheffena

***Abstract*— We present the design and development of a combined octagonal and square-shaped coplanar waveguide (CPW)-fed nanosilver inkjet-printed on Kapton polyimide-based flexible antenna sensor for liquid acetone/water detection which is the first of its kind. Sensing was performed by monitoring the resonant frequency and its corresponding amplitude of the reflection coefficient. Our experimental results show that the antenna sensor is able to distinguish between water and acetone, and it can also respond to varying concentration levels of acetone. The overall size of the antenna sensor is $0.564\lambda_0 \times 0.627\lambda_0 \times 0.001175\lambda_0$, where λ_0 is calculated at 4.7 GHz. The proposed sensor can operate under deformed conditions, making it suitable for sensing near a liquid mixture (acetone-water) by wrapping around the sample holder surface. The results without materials under test show a 10-dB impedance bandwidth between 4.61 GHz and 4.81 GHz in simulations, and from 4.42 GHz to 4.86 GHz in measurements. The simulation results also show a peak realized gain of 4.44 dBi with a maximum total efficiency of 92.8%. In comparison, the measured gain of 4.12 dBi at 4.7 GHz with a maximum total efficiency of 76.5%. Furthermore, experimental results considering the materials under test show that the resonant frequency of the sensor was at 4.63 GHz and 4.54 GHz without– and with– 100% acetone presence in liquid mixtures, respectively. Thus, the proposed antenna sensor has great potential in non-contact liquid acetone sensing applications, paving the way for antenna-based liquid sensing solutions.**

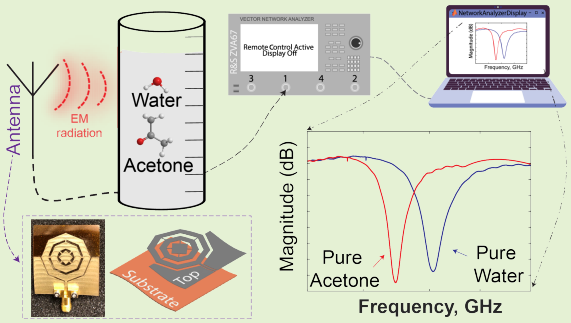

***Index Terms*— Flexible antennas, flexible antenna sensor, antennas, antenna sensor, acetone, 5G, sub-6 GHz, inkjet-printed, nanosilver.**

I. Introduction

ACETONE is a commonly used solvent in industry, laboratory, medical, cosmetic, and household applications due to its solvency properties and ability to evaporate quickly [1], [2]. However, high levels of acetone in the body can be toxic [3], [4]. It is also highly volatile and has a low molecular weight, making it readily transferable to air and water. It has been found to be present in the water supplies, raising concern about potential health hazards when mixed with water [5]–[7]. Therefore, the development of sensors for monitoring acetone in liquid mixtures has become essential in various fields, including domestic drinking water, biomedical research, environmental monitoring, and industrial process control.

Microwave sensors have been widely used in conjunction with electrochemical or chemo-resistive sensors for acetone detection, enabling the monitoring and control of the composition and concentration of both liquid and gaseous forms [3], [8]–[10]. They possess the unique capability to absorb and desorb a target analyte without relying on additional energy sources [11]–[14]. Instead of using a resonator to construct microwave sensors [15]–[17], an antenna can be designed to act as a sensor as it can transmit/receive signals in addition to sensing [18], [19]. Antenna sensors use the propagation characteristics of electromagnetic (EM) waves within a specific frequency range for sensing purposes [20]–[22]. They are used in different sensing applications such as temperature [23], strain [24], and liquid concentration estimation [25].

In recent years, flexible antenna systems have emerged as a viable component in wireless communications [26], [27]. In contrast to brittle and rigid substrates, flexible substrates (e.g., paper, polyimide, polyethylene, and plastics) offer an attractive and feasible alternative for state-of-the-art electronics [28]. With its many advantages including drop-on-demand and non-contact properties, good production adaptability, fast fabrication turnaround, low cost, and roll-to-roll compatibility—inkjet printing (IJP) technology is widely used. By eliminating the need for costly masks and material waste associated with the conventional subtractive manufacturing process, it provides an

This work was supported by the Research Council of Norway under project number 324061.*(Corresponding author: Yu Dang.)*

The authors are with the Faculty of Engineering, Norwegian University of Science and Technology (NTNU), 2815 Gjøvik, Norway (e-mail: kabir.hossain@ntnu.no; yu.dang@ntnu.no; michael.cheffena@ntnu.no).

alternative for the rapid and low-cost production of integrated circuits [29], [30]. In fact, in the existing body of research, a multitude of IJP based sensors have been proposed for sensing applications, e.g., human body temperature monitoring [31], [32], gaseous analytes detection [33]–[35], pressure [36], [37], strain [38], [39], humidity [40], [41], and biological samples characterisation [42], [43]. Furthermore, the versatile IJP technology has demonstrated its effectiveness in liquid sensing applications, such as Gugliandolo *et al.* [44] reported a sensor stracture using two-capacitive coupled split-ring resonators-based IJP to sense ethanol concentration.

The polyimide-based Kapton substrate has been used in [45] due to its exceptional electrical, mechanical, chemical, and thermal properties. Most research on metal deposition by inkjet printing has focused on silver because of its high conductivity, cost-effectiveness, and resistance to oxidation [46], [47]. When compared to other types of ink (e.g., copper, gold, nickel), silver surpasses copper and nickel as it remains stable without forming oxides [48], [49] and does not require complex sintering equipment [50]–[53]. Additionally, in comparison to gold, silver ink is much cheaper [54], [55]. When considering thin substrates (such as Kapton) for the design of an antenna sensor, the coplanar waveguide (CPW) approach appears to be the best option [56]. The CPW-fed technique has also been widely used by the antenna research community to achieve wide bandwidth [30], [57]–[59]. However, achieving a narrow band is necessary for liquid detection as it improves the sensitivity of the sensor. To emphasise this point, frequency domain sensors are preferred for use in narrow bandwidth applications [21], [60]. Furthermore, in a resonance-based sensor (e.g., antenna-based sensor), a narrower bandwidth can ensure a more accurate measurement. This is because the dense fringing field on the sensor resulting from a narrow bandwidth can be highly sensitive to the material under test [61], [62]. Also, the sensing performance of the microstrip sensor is closely related to its structural characteristics [63].

In addition to a narrow bandwidth, the choice of operating frequency band is critical to antenna sensor design. However, diverse works in the literature have utilised various frequency bands to design microwave sensors. Although there is no consensus on the optimal frequency band for sensor development, the choice of frequency should be based on both the requirements of the application and its future prospects. Consequently, the selected operating frequency is primarily determined by considerations related to communication bands. In fact, the fifth generation (5G) sub-6 GHz could be one of the promising candidates [64]. The increasing demand for high data rates in recent years has led researchers to find a viable alternative, with 5G sub-6 GHz frequency bands being adopted in many countries [65]. According to 3GPP, the 5G sub-6 GHz frequency bands are classified under FR1, more specifically they are designated by the numbers n77 (3.3–4.2 GHz), n78 (3.3–3.8 GHz), and n79 (4.4–5.0 GHz) [66]. Among the FR1 frequency bands, n79 has become one of the most promising candidates for future mobile applications and has been extensively studied by many researchers [67], [68]. We can also use this frequency band for antenna sensor development, paving the way for the proposed sensor to be used in existing wireless systems [14], [69].

The most commonly used microwave sensors for liquid detection rely on resonators [60], [70]–[75]. However, these sensors lack communication and contactless sensing capabilities. While Zhu *et al.* [76] investigated antenna-based sensors utilising microfluidic cavities integrated into antennas. However, these reported sensors require contact with the liquid analyte for sensing, making immediate reuse difficult and affecting performance due to residues from previous experiments. There are also a limited number of inkjet-printed sensors that have been proposed. Dai *et al.* [77] developed a flexible microwave sensor using a spoof surface plasmons resonator printed on Polyethylene terephthalate, assessing response only with air, water, or ethanol. In another study [44], a split-ring resonator-based microwave sensor was inkjet printed on a rigid FR4 substrate, which lacks flexibility but it possesses contactless sensing capabilities.

This paper proposes a nanosilver inkjet-printed on Kapton polyimide-based conformal flexible antenna sensor in n-79 band of 5G sub-6 GHz. To date, limited study on inkjet printed flexible material (e.g., Kapton polyimide) based designs have been reported [78]. In [79], an artificial magnetic conductor-loaded Kapton-substrate-based RFID tag antenna at 2.45 GHz was designed. However, in the design process, 9 mm thick foam was used, and hence the overall antenna size is bulky. Conductive graphene on Kapton-based inkjet printed quasi-Yagi–Uda antenna with low gain and efficiency was reported in [80]. Moreover, Khaleel *et al.* [57], and Wang *et al.* [58] developed flexible CPW-fed inkjet printed antennas for wideband applications. Compared to state-of-the-art wideband CPW-fed antenna designs considering flexible thin substrates, our contribution lies in presenting a pioneering flexible narrowband CPW-fed antenna sensor fabricated using IJP technology while upholding efficiency, marking the inaugural achievement of its kind to the best of our current knowledge. Contactless permittivity measurement of liquid under test (i.e., acetone-water mixture) was performed by analysing the reflection coefficient from the sensor. The sensor can respond to the minimal concentration (as low as 20%) of acetone in water. The novel designs can also be used to create a portable sensor instrument that can be conveniently used to monitor the presence of acetone in liquid mixtures in a wide range of applications, including domestic water supply. The flexibility also allows the sensor to be attached to the surface of the sample holder, which would provide an accurate sensing without having a direct contact with the liquid under test.

II. Flexible Polyimide-Based Antenna Sensor Design

A polyimide-based flexible antenna sensor was modelled and simulated using Computer Simulation Technology (CST) Microwave Studio Suite (MWS) in a time-domain solver over the frequency range from 3.5 GHz to 5.5 GHz. The substrate material used was 75 μm thick DuPont^{TM} Kapton$^{®}$ HN with a dielectric constant of 3.4, and a loss tangent of 0.002. Meanwhile, silver nanoparticles (AgNPs) were used as the radiator of the antenna sensor.

Fig. 1 depicts the proposed antenna sensor designed by combining two octagonal and a square-shaped patch. Firstly, this shape was chosen by considering a coplanar waveguide-fed in our design which helps to reduce the fabrication complexity, shows optimum performance and makes it suitable for inkjet printing. Secondly, the octagonal-shaped patch of split-ring resonators acts as a *LC* resonator—contributing to a lower resonant frequency. This in turn helps to miniaturise the overall structure of the antenna sensor [81], [82]. The combined octagonal and square structure also helps to improve the electromagnetic current flow, which is discussed in more details in the following subsection. The tuning of the antenna resonant frequency can be achieved by accurately modelling the gaps present in the design, namely those between the octagonal and square geometries [63]. In addition, Kapton polyimide was used in our design due to its excellent electrical, thermal, chemical, and mechanical properties. Kapton is also a suitable substrate for inkjet printers to print conductive nanosilver inks. Finally, the chosen antenna sensor design allows for impedance matching at the chosen frequency band and for maximum gain and radiation efficiency. In addition, the proposed design offers a narrow operating bandwidth at the frequency of interest, as opposed to a wide band, making it suitable for use in liquid acetone sensing in water. The overall dimension of the antenna sensor is $36 \times 40 \times 0.075$ mm^3 ($0.564\lambda_0 \times 0.627\lambda_0 \times 0.001175\lambda_0$, where λ_0 is the free space wavelength at 4.7 GHz). All dimensions are tabulated in Table I.

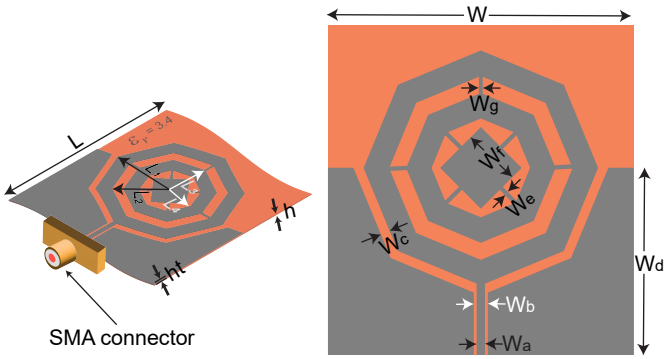

Fig. 1. Schematic diagram of the proposed antenna sensor.

TABLE I
ANTENNA SENSOR PARAMETERS

Parameter	W	L	L_1	L_2	L_3	L_4	W_a	W_b
Value(mm)	36	40	13.5	10	8.5	5	1	1.6
Parameter	W_c	W_d	W_e	W_f	W_g	h	ht	–
Value(mm)	1.7	22	0.5	3.8	0.5	0.075	0.0175	–

A. Antenna Sensor Design Geometry and Configurations

Fig. 2 shows the antenna sensor design analysis and optimisation process. We simulated and analysed the surface current distribution at 4.7 GHz where the colour represents the current intensity—of the antenna designs to gain further insight into its working principles. A combined octagonal and square resonator was considered as the radiating element of the antenna design.

Fig. 2(a) shows the antenna design with a full ground plane, where the chosen radiating element helps to perturb a strong surface current concentration at the inner edges of the octagonal-shaped radiator. Furthermore, a strong electromagnetic coupling was realised due to the extremely small distance between the top plane (radiating element) and the ground plane. The strong electromagnetic coupling causes a significant impedance mismatch, as can be seen from the reflection coefficient (S_{11}) results shown in Fig. 2(a). In addition, we also observed a similar phenomenon for the partial ground plane design (shown in Fig. 2(b)). However, adopting a partial ground plane contributed to a slightly lower mutual coupling effect compared to a full ground plane resulting in a better S_{11} performance as shown in Fig. 2(b). Fig. 2(b) also shows that strong mutual coupling occurs where the ground plane is located. This means that the feed line area has the most electromagnetic coupling, which can also be seen from the surface current distribution. A coplanar waveguide-fed approach was further adopted in Fig. 2(c)—where a partial CPW plane was used. At this stage, a capacitive effect was realised between the microstrip line and the coplanar plane, contributing to the impedance matching, as evidenced by a 10-dB bandwidth improvement over the previous steps. The design was further extended to a full CPW plane on the top plane as shown in Fig. 2(d). In contrast, a full CPW plane created a strong coupling with the radiating element. Similarly, the step in Fig. 2(d) does not provide a better S_{11} impedance result. The design was further optimised as shown in Fig. 2(e). The optimised design achieves a balance between surface currents and the resonance of the sensor. This balance results in an optimum coupling effect between the CPW plane and the radiating element, leading to a significantly improved 10-dB impedance bandwidth.

B. Fabrication Process of the Proposed Antenna Sensor

The detailed fabrication procedures are depicted in Fig. 3. In the first step, we exported the Gerber file of the antenna sensor design from CST MWS. Then in the second step, the Gerber file was converted to a 1-bit Bitmap image with ACE® 3000 (from Numerical Innovations Inc., Henderson, Nevada, USA), where the image resolution was setup up according to the print drop space. Then, the Bitmap file was uploaded to the DMP-2850 printer (from Fujifilm, Greenwood, Indiana, USA) and saved as a pattern file—after confirming the dimension, and drop space. Then in step 4, the Metalon® JS-A291 nanosilver ink (from Novacentrix, Austin, Texas, USA) was placed in an ultrasonic shaker for 5 min to eliminate any aggregation and make the ink more homogeneous. Chemical compositions of the AgNPs ink are also shown in step 4, which consists of water, diethylene glycol and a non-hazardous polyurethane dispersion along with the Ag nanoparticle [83]. In the fifth step, the ink was filtered with a 0.2 μm PTEF filter attached to the syringe to avoid any nozzles clogging. Then 1.5 mL ink was filled to the cartridge and the pattern was printed at room temperature. Since drop space has a considerable

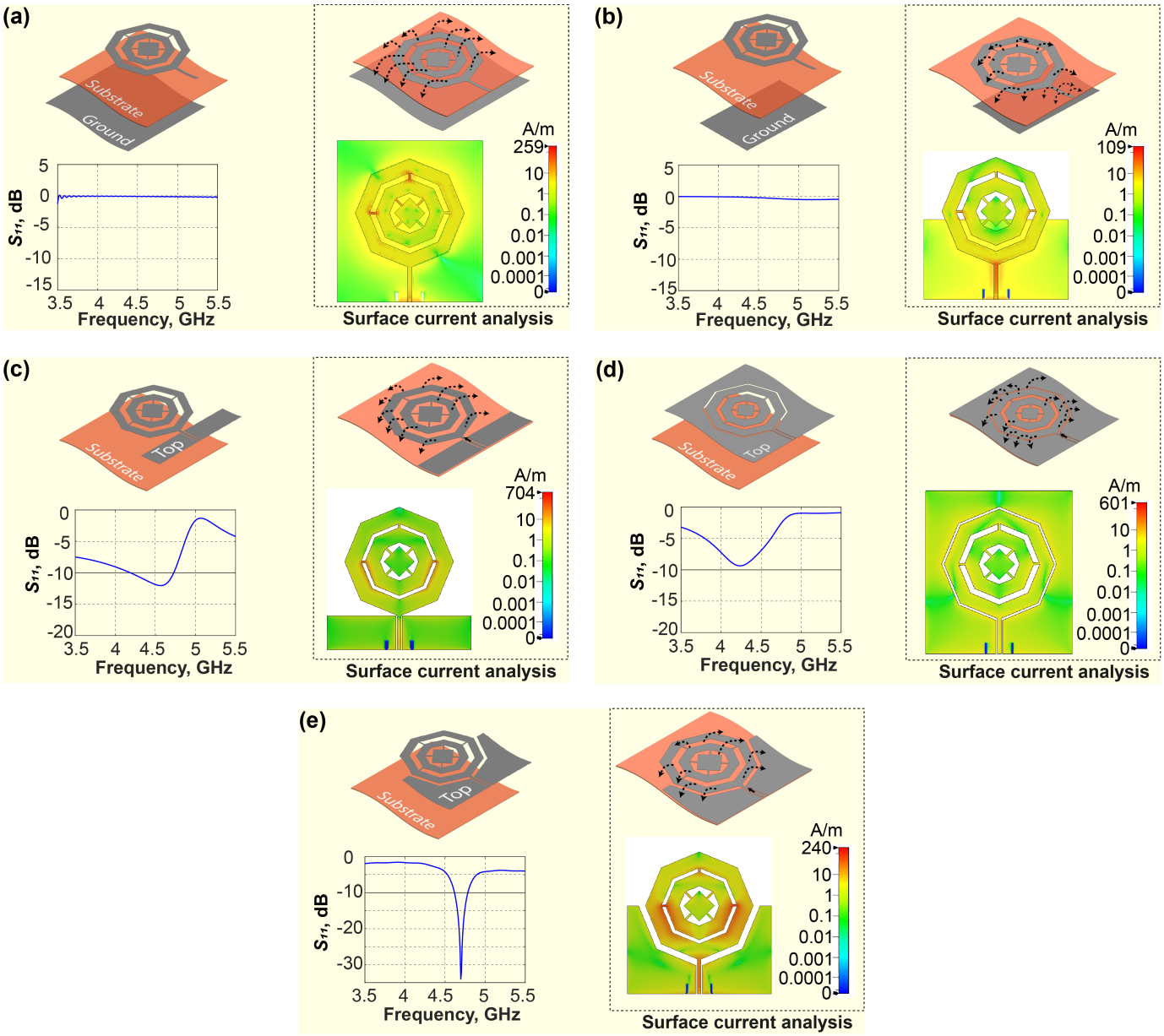

Fig. 2. Antenna sensor design analysis and evolution process in this study. Antenna sensor design considering (a) full ground plane, (b) partial ground plane, (c) partial CPW plane, (d) full CPW plane, and (e) optimised design with a CPW plane.

influence on the final resolution and conductivity, we tried 5 μm, 10 μm, and 15 μm, and we found that 10 μm offered the best result in terms of both conductivity and resolution. After inkjet printing, we sintered the print in a convection oven at a temperature of 200 °C for 5 min to bond Metalon® JS-A291 nanosilver ink to DuPont™ Kapton® HN substrate. This procedure generates long-lasting conductive pathways, improving flexibility while preserving efficiency [84], [85]. Sintering guarantees strong ink adhesion, minimising the likelihood of detachment during bending and maintaining low resistance to enhance antenna sensor efficiency [45], [84], [86]. Nevertheless, precise sintering time and temperature regulation are imperative to prevent any harm to the substrate, and ensuring uniformity is vital for maintaining consistent conductivity [86], [87]. Afterwards, a SMA connector (from Rosenberger, Mfr. Part No.: 168322, GmbH, Germany) was assembled to the printed antenna sensor in the final step. The fabricated prototype of the proposed antenna sensor is shown in step 7 (the last step).

III. Results of the Proposed Antenna Sensor

The simulated and measured reflection coefficient result of the proposed antenna sensor is shown in Fig. 4. The simulated result shows a 10-dB impedance bandwidth of 200 MHz (4.61–4.81 GHz) with VSWR$<$1.06. We measured the antenna sensor's S_{11} using a Vector Network Analyzer (VNA, ZVA 67, Rohde and Schwarz) to ensure that the simulated results were accurate. The measured result shows a 10-dB impedance bandwidth of 440 MHz (4.42–4.86 GHz), which is greater than the simulated result. The discrepancy between the measured

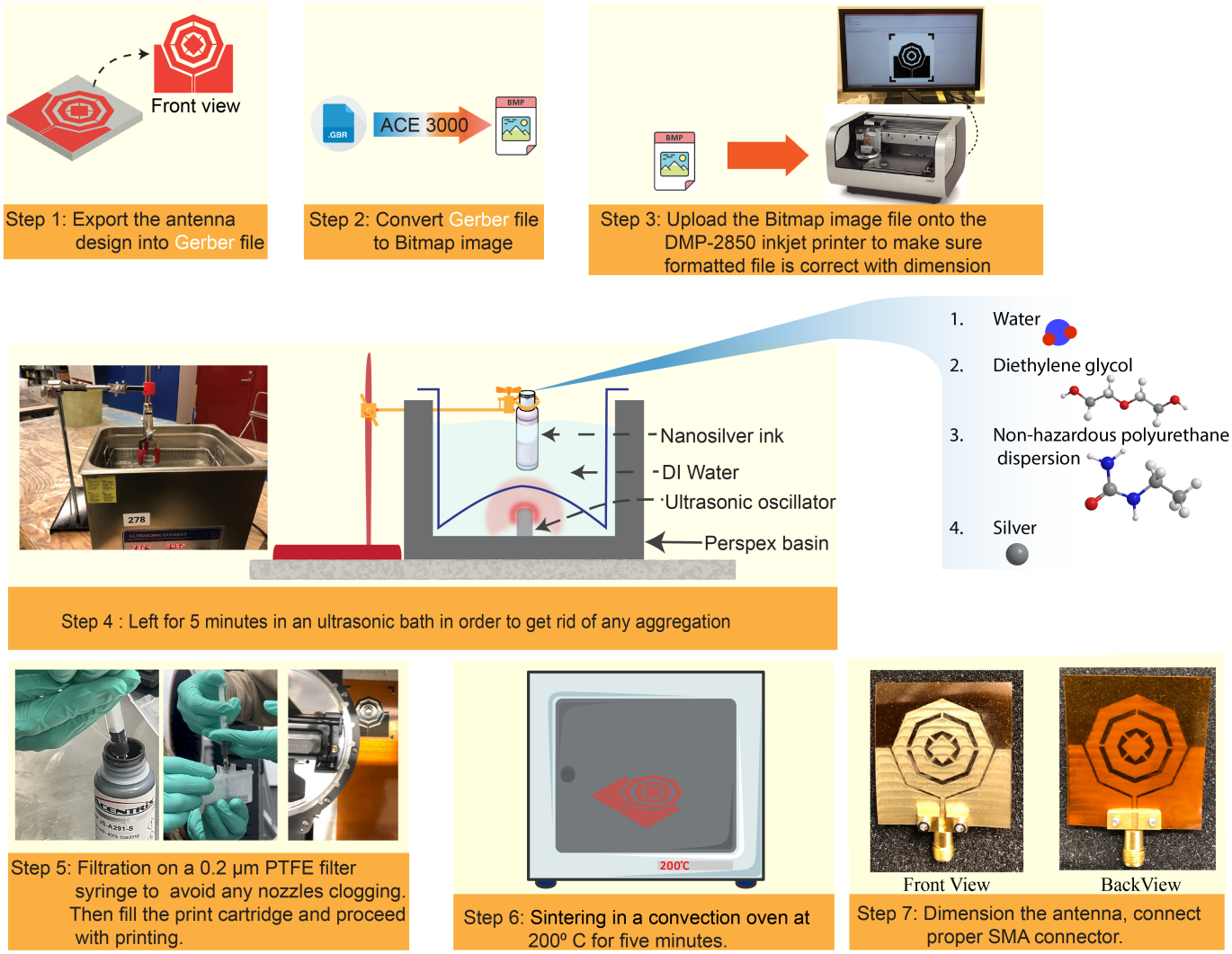

Fig. 3. Antenna sensor fabrication steps and procedures in this study.

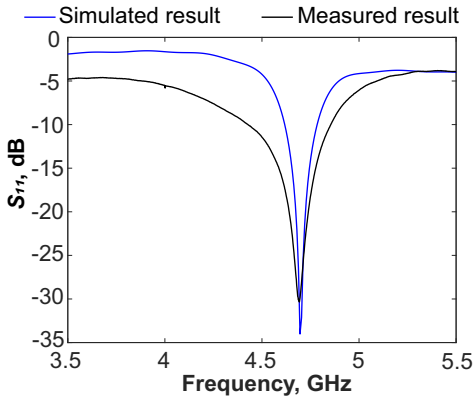

Fig. 4. Simulated and measured S_{11} results of the proposed antenna sensor.

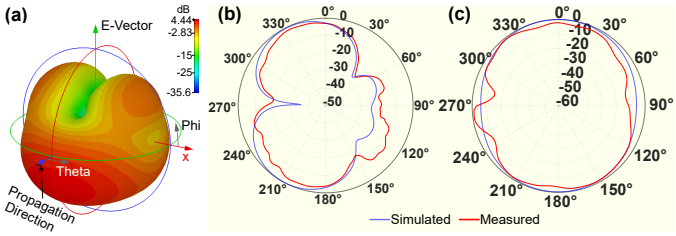

Fig. 5. (a) 3D radiation pattern, and normalised radiation pattern at (b) E (yz)–plane and (c) H (xz)–plane of the proposed antenna sensor.

and simulated impedance bandwidth could be explained by differences in fabrication accuracy and soldering procedures. Simulation accuracy, however, can be increased by improving precise material modelling and optimising boundary conditions. Thus, perfect impedance matching was achieved within the frequency of interest meaning that we can potentially use this design for various mobile applications in the 5G sub-6 GHz regime.

Fig. 5(a) shows simulated 3D radiation pattern, and Figs. 5(b) and 5(c) illustrate simulated and measured normalized radiation pattern results of the proposed antenna sensor at 4.7 GHz for E (yz)– and H (xz)–planes, respectively. The radiation pattern observed in the E–plane is bidirectional, while the H–plane shows omnidirectional patterns for both simulations and measurements. The observed bidirectional

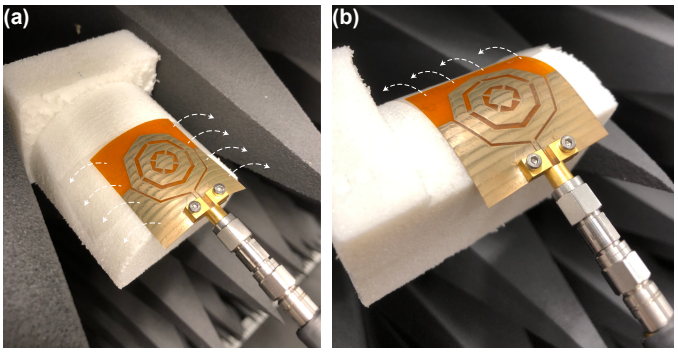

Fig. 6. Photograph of experimental bending along the (a) x–axis, and (b) y–axis.

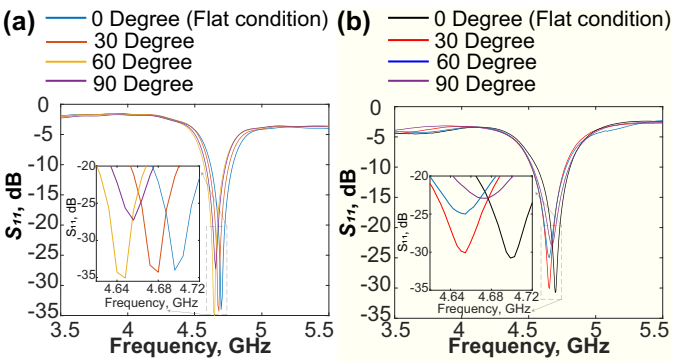

Fig. 7. The effects of bending the antenna sensor along the x–axis: (a) simulated results for various radii, and (b) measured results with approximate bending radii.

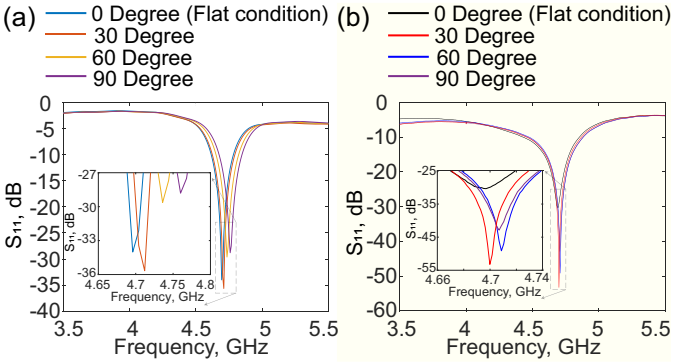

Fig. 8. The effects of bending the antenna sensor along the y–axis: (a) simulated results for various radii, and (b) measured results with approximate bending radii.

radiation pattern in the E–plane indicates that the antenna sensor shows varying radiation intensity in two opposing directions within the vertical plane. Conversely, the omni-directional radiation pattern in the H–plane refers to the radiation pattern's consistency in all directions within the horizontal plane. The bi-directional radiation on E–plane and omnidirectional radiation on H–plane of our antenna sensor can enable communication even if blocked by a liquid sample under test. Knowing radiation patterns in both E– and H–planes helps define the antenna sensor coverage [88] and calculate the link budget [89] in practical applications. This knowledge can also aid in system-level optimisation for sensor network deployment and helps mitigate interference in crowded electromagnetic environments, ensuring robust performance. Moreover, the simulated result shows a peak gain of 4.44 dBi at 4.7 GHz, while the measured results show a 4.12 dBi gain. The maximum total efficiency achieved at 4.7GHz is 92.8% in the simulation and 76.5% in the measurement. The observed 0.32 dBi difference in gain between simulation and measurement results can be attributed to inherent dielectric and conduction losses in the substrate material, worsened by SMA connector losses [90]. Additionally, the flexible nature of the antenna during measurements led to deviations from the theoretically flat configuration predicted by simulations. To address this, maintaining the antenna in an ideal flat condition during measurements is crucial. Furthermore, substrate thickness plays a role in radiation efficiency; reducing thickness may increase conduction and dielectric losses [91]. To enhance simulation accuracy and measurement consistency, employing a high-quality, low-loss tangent substrate material is recommended [92]. Implementing these measures will likely minimise disparities, improving the accuracy of the antenna's performance characterisation in both simulation and measurement scenarios.

A. Deformation Analysis

If the antenna sensor is made of a flexible material, it is more likely to have a physical deformation effect (due to stretching or bending), which results in changing the EM properties of the antenna sensor. This causes an unwanted impedance mismatch [93]–[98]. Therefore, we evaluated the S_{11} result of the proposed antenna in the presence of different bending radii.

The experiment setup of deformation measurement along the x-axis and y-axis is shown in Fig. 6. In this setup, a series of Polyethylene Terephthalate foam (PET foam, AIREX® T10.100, 3A Composites Core Materials, Switzerland [99]) cylinders with different diameters were customised with the aid of turning-lathe machine. The radius of the cylinders were determined according to the different bending angle (approximately 30°, 60° and 90°) [100]–[102]. Due to the fact that the permittivity of this foam is very similar to that of air, we disregarded the foam support's influence on the antenna sensor.

Fig. 7(a) shows simulated results, and Fig. 7(b) shows measured results for different banding conditions along the x–axis. Both simulated and measured findings show a frequency shift toward a lower frequency. Fig. 7(a) also indicates simulated resonant frequency shift is on average 50 MHz. Furthermore, Fig. 7(b) shows a similar trend to the simulation, but it exhibits an average 60 MHz shift toward higher frequency. Also, the measurement shows a wider 10-dB impedance bandwidth, from 4.65 GHz to 4.71 GHz, which is ultimately within the n79 band.

Furthermore, we also carried out bending analysis at the y-axis for both simulation and measurements which are shown in Fig. 8. Simulated bending analysis results—which are shown in Fig. 8(a)—indicate a slight resonant frequency shift toward higher frequency with, on average 35 MHz. Fig. 8(b) shows

measured bending analysis results with a minor frequency shift—where the average shift is less than 10 MHz. Hence, both simulation and measurement show a similar trend, considering bending analysis indicates a good agreement with both simulations and measurements.

We conducted a detailed investigation into the physical deformation of the proposed antenna sensor to reveal its durability and adaptability, key attributes that significantly influence its performance in challenging conditions. Based on our observations, the sensor can consistently maintain a stable response, highlighting its durability under adverse situations. This suggests that the sensor can exhibit balanced sensitivity across its measurements, particularly in liquid acetone/water sensing. Also, the flexibility allows the sensor to be attached to the surface of the sample holder, which would provide an accurate measurement result in a non-invasive manner—enhancing its versatility in liquid sensing applications. The sensor is specifically designed for the non-contact detection of liquid acetone and water, showcasing its potential for adaptability in various fields, such as wireless RF systems, sensor technology, and emerging RF/microwave applications.

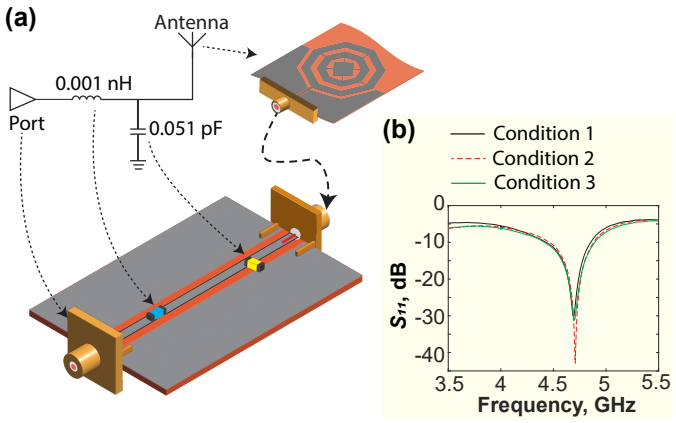

Fig. 9. (a) Illustration of impedance matching circuit with a corresponding test board—where series inductor value is 0.001 nH, and parallel capacitor value is 0.051 pF. (b) Performance evaluation of the impedance matching network, where Condition 1: ideal measured S_{11} result of the antenna sensor, Condition 2: impedance mismatch condition while the antenna was deformed with a bending radius approximately 60° along with the x–axis in real life measurement scenario, and Condition 3: impedance matched condition for the Condition 2 with considering matching network.

B. Impedance Matching

Numerous studies have reported experiencing impedance mismatched effects due to bending (while considering flexible material) or fabrication error [26]. Mindful of the fact that, this problem can be solved with a proper LC impedance matching circuit to ensure efficient power transfer between the antenna and measurement equipment. While reading this paper, some readers may be interested to know what would happen if we do not achieve the expected antenna performance (due to bending or other effects that can cause impedance mismatch). The readers in this concern can find more information related to the RF-front end, involving impedance matching network and antennas, in [103]–[106].

Although outside the main scope of this manuscript, we provide a brief insight into this kind of problem and its solution related to impedance mismatches. For demonstration purposes, we suppose the antenna was bent 60° at the y–axis (for the worst-case scenario) as considering measurement results—refer to Fig. 8(b). Fig. 9(a) shows an impedance-matching circuitry with a corresponding test board considering a series inductor (0.001 nH) and a parallel capacitor (0.051 pF). Thus, Condition 1 in Fig. 9(b) represents the ideal condition for the measured results and where the antenna/sensor is intended to radiate. We suppose our antenna is in the mismatched state shown in Condition 2. After adopting the impedance matching circuitry for Condition 2 (which is shown in Fig. 9(a)), we observed that the attainable result—shown in Fig. 9(b) Condition 3—is in good agreement.

IV. Contactless Liquid Acetone/Water Detection

The sensing procedures are shown in Fig. 10. First, we calibrated the sensor. As part of the calibration procedure, we recorded five readings and averaged them—to make sure the measured data was accurate—by considering it in the vicinity of the empty liquid sample holder, without liquid under test (LUT). In fact, the sensor was considered in the bent condition. The resonant frequency could show cross-sensitivity to the shape (bending) of the antenna, which would lead to measurement errors. However, calibration strategies helped to avoid these errors taking into account the deformation of the antenna sensor around the sample holder during the measurements. The calibration result was taken as the reference for future comparisons. A micropipette was used to add a specific amount of acetone and distilled water to a small vial (from Sigma-Aldrich®, USA, with a total capacity of 11 cm^3 [109])—as shown in Fig. 10(a). Throughout the contactless liquid acetone/water detection with our proposed antenna sensor, we maintained a constant volume at 10 cm^3 for all liquid mixtures with different concentrations. Water and acetone solutions of varying concentrations were added to the liquid under test and measured numerically by the proposed sensor to determine the frequency shift. The acetone content was chosen to range from 0% (100% water) to 100% (0% water) with a step of 10%. The proposed antenna sensor was touched the outer surface of the small vial with a bent condition and the VNA measured the reflection coefficient. To minimise any possible interference (due to human movement), the experimental equipment was shielded using a microwave absorber, as shown in Fig. 10(b). Microwave absorbers isolate the antenna from the outside environment by reducing unwanted reflection/transmission and interference, thus ensuring reliable measurements. In addition to eliminating the influence of antenna and cable movement, a small box was used as a holder to fix the cable and antenna, and this box was opened during the experiment. The VNA was also connected to a laptop computer via a LAN cable and programmed using MATLAB software to measure data without interrupting the process.

The theory behind the liquid mixture adopted in this study is that different volume fractions of acetone in DI water lead to variations in the relative permittivity of the mixture. To

This article has been accepted for publication in IEEE Sensors Journal. This is the author's version which has not been fully edited and
content may change prior to final publication. Citation information: DOI 10.1109/JSEN.2024.3361911

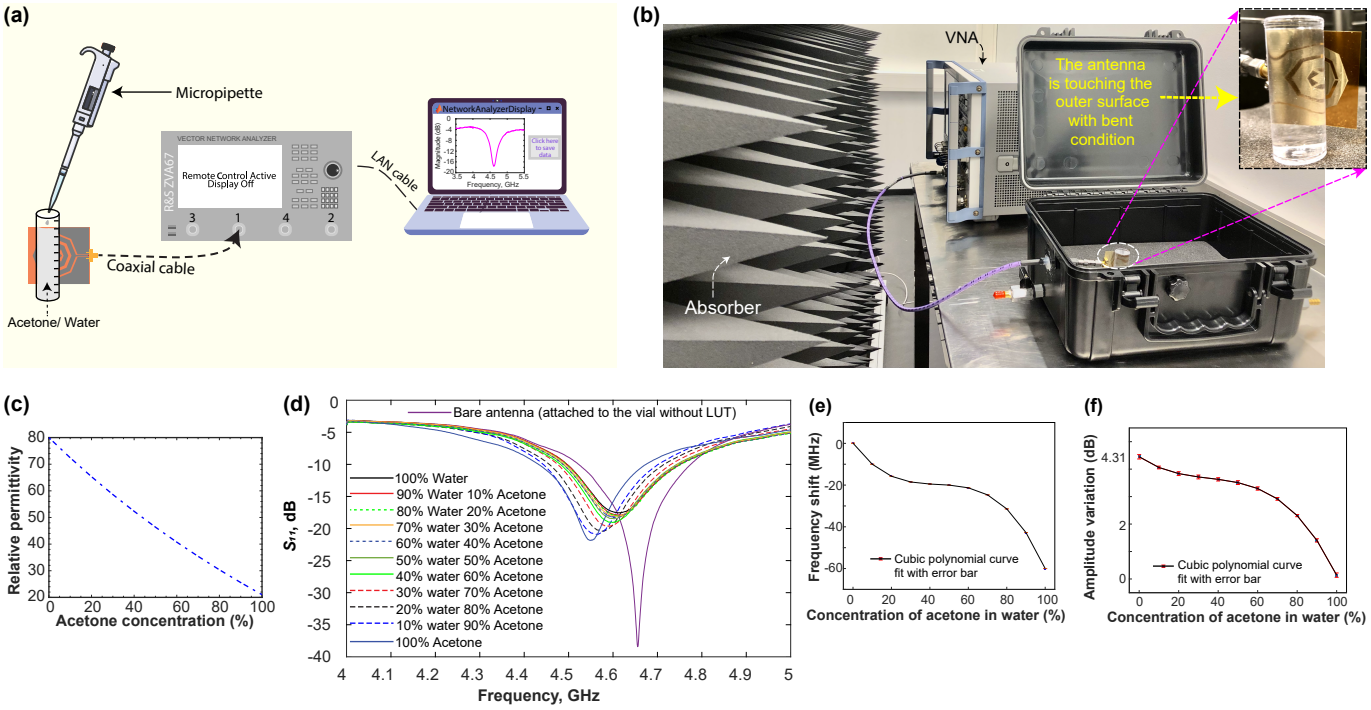

Fig. 10. (a) Graphical presentation of the experimental setup. (b) Photographic of the experimental setup where the proposed antenna sensor was connected to a VNA and data was recorded using a computer via MATLAB software. (c) Relationship between acetone concentration and relative permittivity in the liquid mixture of the experiment. Measured responses of the proposed antenna sensor: (d) $\boldsymbol{S_{11}}$ as a function of frequency for different acetone/water concentrations; and its corresponding (e) scatter plot with error bar and cubic polynomial curve fitting relation between acetone concentration and frequency shift, and (f) scatter plot with error bar and cubic polynomial curve fitting relation between acetone concentration and amplitude variation.

show intuitively how the relative permittivity of the binary mixture changes with the concentration of acetone, a widely used Maxwell-Garnett model [110], [111] can be considered, which can be calculated mathematically using (1),

$$\varepsilon_{eff} = \varepsilon_{r_1} + 3\,|m|\,\varepsilon_{r_1} \cdot \frac{\varepsilon_{r_2} - \varepsilon_{r_1}}{\varepsilon_{r_2} + 2\varepsilon_{r_1} - |m|\,(\varepsilon_{r_2} - \varepsilon_{r_1})} \quad (1)$$

where ε_{r_1} and ε_{r_2} are the relative permittivities of DI water and acetone, which are 80 and 21, respectively [112], [113], and m is the concentration of acetone in DI water. Then again ε_{eff} is the relative permittivity of the mixture, which is plotted in Fig. 10(c). As we can see, as the concentration of acetone increases, the permittivity of the mixture gradually decreases because the permittivity of acetone is lower than that of DI water.

Fig. 10(d) shows the measured S_{11} data for different mixtures. The 10-dB impedance bandwidth for the bare antenna was measured to be 251 MHz. When introducing DI water and acetone, the 10-dB impedance bandwidths were observed to be 255 MHz and 241 MHz, respectively. Compared to the empty vial, the presence of acetone resulted in an average 4.15% decrease in bandwidth, while an approximate 1.6% increase in the average bandwidth was observed as the water percentage increased within the mixture. It also shows a noticeable change in both amplitude and frequency compared to reference frequency which helps trace the acetone level in the water. The reference frequency is at 4.66 GHz with an amplitude of –38.43±0.06 dB. Considering a 10% acetone concentration, the resonant frequency shifted to 4.62 GHz with an amplitude of –18.95±0.05 dB, which corresponds to a 40 MHz resonant frequency shift, and about 20.88 dB change in amplitude. It can also be seen from Fig. 10(d) that a higher concentration of acetone causes the S_{11} to shift towards a lower frequency range. The resonant frequency of the sensor was at 4.61 GHz and 4.55 GHz without (0%) and with (100%) acetone presence in liquid mixtures, respectively. Therefore, the proposed antenna sensor can be used to quantitatively discriminate the concentration of the acetone-water mixture.

Sensitivity and limit of detection (LoD) are the two most important indicators of sensor performance. In this study, we established a quantitative relationship between the acetone concentration and the observed variations in the S_{11} from our antenna sensor. Fig. 10(e) and Fig. 10(f) show the variations in resonance frequency and amplitude, respectively, as the acetone concentration in DI water was varied. We conducted thorough experiments where the sensor was exposed to a range of known acetone concentrations in controlled settings. By recording the sensor's response to these concentrations, we established a quantitative relationship between the acetone concentration and the reflection coefficient of the antenna sensor.

We applied a cubic polynomial fitting curve to further analyse the data shown in Fig. 10(d) considering 0–100% acetone concentration in DI water. The selection of cubic polynomial fitting was motivated by the need to effectively capture the curvature in the data. As illustrated in Fig. 10(e) and Fig. 10(f), the data points closely follow the cubic polynomial curve, sug-

TABLE II
A COMPARISON OF THE MEASUREMENTS OF THIS WORK WITH OTHER RELEVANT WORKS BASED ON THEIR KEY PARAMETERS

Ref.	Sensor Type	Operation freq. (GHz)	Sensitivity (kHz/ percentage)	Com. Cap.	Measured gain	Measurement setup	Flex.	IJP	CSC	Sensor size (mm^3)
[44]	Split ring resonators	2 – 3	188	No	NA	Water and ethanol	No	Yes	Yes	60×20×1.6
[60]	Dielectric resonator	2.45	718	No	NA	Water and ethanol	No	No	No	NA
[70]	SIW cavity resonator	3.16	2600	No	NA	Water and ethanol	No	No	No	20×21×1.27
[71]	SIW resonator	10	900	No	NA	Water and methanol	No	No	No	NA
[72]	Complementary split ring resonator	2	350	No	NA	Water and ethanol	No	No	No	20×25×1.6
[73]	Complementary split ring resonator	2.36	440	No	NA	Water and ethanol	No	No	No	20×28×0.75
[74]	Complementary split ring resonator	2.4	300	No	NA	Water and ethanol	No	No	No	25×35×3
[75]	Split ring resonator	2.1	1100	No	NA	Water and ethanol	No	No	No	28×28×1.9
[76]	Split ring patch antenna	1.33 and 2.55	380	Yes	1.5dBi @1.33 GHz and 5.7dBi @2.69 GHz	Water and acetone	No	No	No	85×85×1.6
[77]	Microwave plasmonic resonator	5.23	NA	No	NA	Water and ethanol	Yes	Yes	No	34×40×2.5
[107]	Metamaterial-based resonator	3.2 and 4.85	610	No	NA	Ethanol and 1–pentanol	No	No	No	30.6×61.4×4.2
[108]	Patch antenna	4.478 – 4.833	117.6	Yes	NA	Ethanol in wine and isopropyl in disinfectant	No	No	No	70×70×1.6
This work	CPW-fed patch antenna	4.42 – 4.86	600	Yes	4.12dBi @4.7 GHz	Water and acetone	Yes	Yes	Yes	36×40×0.075

Com. Cap. = Communication capabilities; Flex.= Flexibility; IJP = Inkjet Printed; CSC = Contactless sensing capabilities

gesting a strong correlation between acetone concentration and resonant frequency shift and amplitude deviation, respectively. The mathematical equations governing these phenomena are denoted as (2) and (3), respectively.

$$y = -0.2127x^3 + 0.2792x^2 - 0.1266x + 4.61 \quad (2)$$

$$y = -11.01x^3 + 11.66x^2 - 4.956x - 17.55 \quad (3)$$

Referring to Fig. 10(e) and Fig. 10(f), the response of the sensor to changes in the volume fraction shows a non-linear trend, a characteristic commonly observed in microwave sensors as shown by previous research studies presented in [71], [108], [114], [115]. In addition to presenting this relationship curve, we incorporated error bars in Figs. 10(e) and Fig. 10(f) to illustrate the uncertainty and variability inherent in our multiple measurements. The short length of these error bars indicates a high level of accuracy and repeatability within these measurements. This enabled us to quantitatively evaluate the sensor's ability to measure acetone concentration levels accurately. Apart from that, Figs. 10(e) and Fig. 10(f) show a maximum change of 60 MHz in frequency and a 4.31-dB change in amplitude. The sensitivity can be calculated using (4),

$$S = \frac{\Delta f}{100} \quad (4)$$

where the Δf is the resonate frequency shift from 0% to 100% acetone in water, which is the 60 MHz in our case, S is the sensitivity [60], [116]. By inserting the values in (4), we can get a sensitivity of 600 kHz/percentage.

Table II presents a comparison of the proposed work with recently published microwave sensors designed for liquid mixture sensing. The liquid sensing systems shown in the table demonstrate a wide range of variations in terms of their diverse topologies, constituent materials, working mechanisms, and operational frequencies. This indicates that comparing them directly is a complex undertaking. Nevertheless, this table offers a comprehensive analysis of various microwave sensors and their efficacy compared to the proposed sensor. The

evaluation primarily concentrates on binary liquid mixtures (e.g., acetone/water mixture) as reported in existing literature. Applying inkjet-printed microwave sensors for monitoring liquid mixtures is a comparatively underexplored field. A study cited as [44] demonstrates the development of an inkjet-printed microwave sensor employing split-ring resonators that obtained a remarkable sensitivity of 188 kHz/percentage. A different study using inkjet printing has reported in [77] yielded no results on sensitivity. Our proposed sensor demonstrates a sensitivity value that is comparable to those that are reported in the table, yet this value is somewhat lower than those that are exhibited by the other sensors cited as [70], [71], [75]. This may primarily be attributed to the fact that our sensor is specifically designed for contactless measurements, particularly for characterising the liquid mixtures within a container (e.g., a vial). In this scenario, the key component that may contribute to the reduced sensor sensitivity is likely the thickness of the container itself. However, despite this consideration, the proposed sensor still showcases commendable performance. Its cost-effective fabrication process, which is achieved with the inkjet-printing technique, renders it an economically viable sensor. Hence, compared to existing liquid sensing systems, our proposed antenna sensor is compact in terms of its electrical size and sensitivity in detecting liquid acetone concentration at room temperature based on radio frequency signals. Also, the proposed antenna sensor is flexible and capable of working under deformation, which would allow the sensor to be attached to the surface of the sample holder, making it ideal for contactless liquid sensing applications.

Besides sensitivity, the limit of the detection is also a crucial characterising metric of a sensor [117]–[120]. In our experiment, we employed a measurement increment of 10%. However, due to the limited variation observed within the 30–70% acetone concentration range, we have considered the worst-case scenario of a 20% change as the practical LoD. Additionally, as demonstrated in Fig. 10(e), a 1% change in acetone concentration in water resulted in a substantial 600 kHz deviation, well within the discernible range of our VNA. Therefore, it is reasonable to conclude that the theoretical LoD may potentially extend as low as 1%.

The proposed antenna sensor utilises commercially available materials, simplifying its fabrication process for improved stability and reproducibility. Detailed procedures, including inkjet printing steps and setup parameters, are provided for easy replication by other researchers. The sensor's stability is validated under different bending conditions. The sensor can also distinguish between acetone and water based on their relative permittivities.

V. Conclusion

We describe the design and development of a combined octagonal and square-shaped patch CPW-fed inkjet-printed flexible antenna for sensing a liquid acetone/water mixture. The proposed antenna sensor provides high sensitivity while operating at room temperature in a laboratory environment. Both simulation and measurement showed that this antenna sensor has an impedance bandwidth of 10-dB between 4.61 GHz and 4.81 GHz. It also has a measured peak realized gain of approximately 4.12 dBi with an efficiency of 76.5%. In addition, the antenna sensor has an omnidirectional radiation pattern in the H plane and a bidirectional radiation pattern in the E plane. Besides, the sintering process of the nanosilver ink is enabled by the Kapton substrate, resulting in the flexibility, compactness, light weight, robustness, and good radiation characteristics of the proposed design. Antenna sensors such as the one proposed in this study have great potential in future conformal and flexible electronic systems. It can be fabricated from advanced materials and can be used for a wide range of wireless applications in the 5G sub-6 GHz n79 band regime. Overall, the proposed design can be used in sensing and/or communication applications, making it a valuable component for sensor networks. As such, it opens up a new horizon for antenna sensor based liquid sensing technologies with potential applications in acetone sensing in cosmetics and personal care products, industrial process control, wastewater treatment, and safety and hazard detection. In future research, we aim to enhance our capabilities to detect more complex conditions, such as varying volumes or different types of liquid mixtures.

References

[1] M. A. El-Naka, A. El-Dissouky, G. Ali, S. Ebrahim, and A. Shokry, "Fluorescent garlic-capped ag nanoparticles as dual sensors for the detection of acetone and acrylamide," *RSC advances*, vol. 12, no. 52, pp. 34 095–34 106, 2022.

[2] R. Abdelghani, H. S. Hassan, I. Morsi, and A. Kashyout, "Nano-architecture of highly sensitive sno2–based gas sensors for acetone and ammonia using molecular imprinting technique," *Sensors and Actuators B: Chemical*, vol. 297, p. 126668, 2019.

[3] Y. Obeidat, A. M. Rawashdeh, A. Hammoudeh, R. Al-Assi, A. Dagamseh, and Q. Qananwah, "Acetone sensing in liquid and gas phases using cyclic voltammetry," *Scientific Reports*, vol. 12, no. 1, p. 11010, 2022.

[4] M. Gupta, P. Chaudhary, A. Singh, A. Verma, D. Yadav, and B. Yadav, "Development of moo3-cdo nanoparticles based sensing device for the detection of harmful acetone levels in our skin and body via nail paint remover," *Sensors and Actuators B: Chemical*, vol. 368, p. 132102, 2022.

[5] E. D. Hudson, K. Okuda, and P. A. Ariya, "Determination of acetone in seawater using derivatization solid-phase microextraction," *Analytical and bioanalytical chemistry*, vol. 388, pp. 1275–1282, 2007.

[6] N. S. Chary and A. R. Fernandez-Alba, "Determination of volatile organic compounds in drinking and environmental waters," *TrAC Trends in Analytical Chemistry*, vol. 32, pp. 60–75, 2012.

[7] E. Fischer, D. J. Jacob, D. Millet, R. M. Yantosca, and J. Mao, "The role of the ocean in the global atmospheric budget of acetone," *Geophysical Research Letters*, vol. 39, no. 1, 2012.

[8] I. C. Weber, H. P. Braun, F. Krumeich, A. T. Güntner, and S. E. Pratsinis, "Superior acetone selectivity in gas mixtures by catalyst-filtered chemoresistive sensors," *Advanced Science*, vol. 7, no. 19, p. 2001503, 2020.

[9] A. Rydosz, E. Maciak, K. Wincza, and S. Gruszczynski, "Microwave-based sensors with phthalocyanine films for acetone, ethanol and methanol detection," *Sensors and Actuators B: Chemical*, vol. 237, pp. 876–886, 2016.

[10] N. Kazemi, N. Gholizadeh, and P. Musilek, "Selective microwave zeroth-order resonator sensor aided by machine learning," *Sensors*, vol. 22, no. 14, p. 5362, 2022.

[11] A. A. Al-Behadili, I. A. Mocanu, T. M. Petrescu, and T. A. Elwi, "Differential microstrip sensor for complex permittivity characterization of organic fluid mixtures," *Sensors*, vol. 21, no. 23, p. 7865, 2021.

[12] M. Abdolrazzaghi, V. Nayyeri, and F. Martin, "Techniques to improve the performance of planar microwave sensors: A review and recent developments," *Sensors*, vol. 22, no. 18, p. 6946, 2022.

[13] N. Kazemi, M. Abdolrazzaghi, and P. Musilek, "Comparative analysis of machine learning techniques for temperature compensation in microwave sensors," *IEEE Transactions on Microwave Theory and Techniques*, vol. 69, no. 9, pp. 4223–4236, 2021.

[14] T. Alam and M. Cheffena, "Integrated microwave antenna/sensor for sensing and communication applications," *IEEE Transactions on Microwave Theory and Techniques*, vol. 70, no. 11, pp. 5289–5300, 2022.

[15] B. D. Wiltshire, T. Zarifi, and M. H. Zarifi, "Passive split ring resonator tag configuration for rfid-based wireless permittivity sensing," *IEEE Sensors Journal*, vol. 20, no. 4, pp. 1904–1911, 2019.

[16] Z. A. Dijvejin, K. K. Kazemi, K. Alasvand Zarasvand, M. H. Zarifi, and K. Golovin, "Kirigami-enabled microwave resonator arrays for wireless, flexible, passive strain sensing," *ACS applied materials & interfaces*, vol. 12, no. 39, pp. 44 256–44 264, 2020.

[17] M. Moradpour, E. Hosseini, M. C. Jain, R. Narang, N. Tanguy, and M. H. Zarifi, "Patterned PEDOT: PSS-enabled organic planar microwave resonator sensors," *Applied Materials Today*, vol. 24, p. 101106, 2021.

[18] R. Kozak, K. Khorsand, T. Zarifi, K. Golovin, and M. H. Zarifi, "Patch antenna sensor for wireless ice and frost detection," *Scientific Reports*, vol. 11, no. 1, pp. 1–11, 2021.

[19] J. D. Adams, S. Emam, N. Sun, Y. Ma, Q. Wang, R. Shashidhar, and N.-X. Sun, "A molecularly imprinted polymer-graphene sensor antenna hybrid for ultra sensitive chemical detection," *IEEE Sensors Journal*, vol. 19, no. 16, pp. 6571–6577, 2019.

[20] W. Y. Chen, X. Jiang, S.-N. Lai, D. Peroulis, and L. Stanciu, "Nanohybrids of a mxene and transition metal dichalcogenide for selective detection of volatile organic compounds," *Nature communications*, vol. 11, no. 1, p. 1302, 2020.

[21] L.-C. Fan, W.-S. Zhao, D.-W. Wang, Q. Liu, S. Chen, and G. Wang, "An ultrahigh sensitivity microwave sensor for microfluidic applications," *IEEE Microwave and Wireless Components Letters*, vol. 30, no. 12, pp. 1201–1204, 2020.

[22] M. Han, Y. Liu, R. Rakhmanov, C. Israel, M. A. S. Tajin, G. Friedman, V. Volman, A. Hoorfar, K. R. Dandekar, and Y. Gogotsi, "Solution-processed ti3c2tx mxene antennas for radio-frequency communication," *Advanced Materials*, vol. 33, no. 1, p. 2003225, 2021.

[23] M. Bhattacharjee, F. Nikbakhtnasrabadi, and R. Dahiya, "Printed chipless antenna as flexible temperature sensor," *IEEE Internet of Things Journal*, vol. 8, no. 6, pp. 5101–5110, 2021.

[24] B. Sindhu, A. Kothuru, P. Sahatiya, S. Goel, and S. Nandi, "Laser-induced graphene printed wearable flexible antenna-based strain sensor for wireless human motion monitoring," *IEEE Transactions on Electron Devices*, vol. 68, no. 7, pp. 3189–3194, 2021.

[25] Z. Li and S. Bhadra, "A 3-bit fully inkjet-printed flexible chipless rfid for wireless concentration measurements of liquid solutions," *Sensors and Actuators A: Physical*, vol. 299, p. 111581, 2019.

[26] M. U. Ali Khan, R. Raad, F. Tubbal, P. I. Theoharis, S. Liu, and J. Foroughi, "Bending analysis of polymer-based flexible antennas for wearable, general iot applications: a review," *Polymers*, vol. 13, no. 3, p. 357, 2021.

[27] L. Su, X. Huang, W. Guo, and H. Wu, "A flexible microwave sensor based on complementary spiral resonator for material dielectric characterization," *IEEE Sensors Journal*, vol. 20, no. 4, pp. 1893–1903, 2019.

[28] L. Yang and M. M. Tentzeris, "Design and characterization of novel paper-based inkjet-printed rfid and microwave structures for telecommunication and sensing applications," in *2007 IEEE/MTT-S International Microwave Symposium*. IEEE, 2007, pp. 1633–1636.

[29] W. T. Li, Y. Q. Hei, P. M. Grubb, X.-W. Shi, and R. T. Chen, "Inkjet printing of wideband stacked microstrip patch array antenna on ultrathin flexible substrates," *IEEE Transactions on Components, Packaging and Manufacturing Technology*, vol. 8, no. 9, pp. 1695–1701, 2018.

[30] S. Ahmed, F. A. Tahir, A. Shamim, and H. M. Cheema, "A compact kapton-based inkjet-printed multiband antenna for flexible wireless devices," *IEEE Antennas and Wireless Propagation Letters*, vol. 14, pp. 1802–1805, 2015.

[31] B. A. Kuzubasoglu, E. Sayar, and S. K. Bahadir, "Inkjet-printed cnt/pedot:pss temperature sensor on a textile substrate for wearable intelligent systems," *IEEE Sensors Journal*, vol. 21, no. 12, pp. 13 090–13 097, 2021.

[32] S. Ali, S. Khan, and A. Bermak, "Inkjet-printed human body temperature sensor for wearable electronics," *IEEE Access*, vol. 7, pp. 163 981–163 987, 2019.

[33] L. Ge, X. Ye, Z. Yu, B. Chen, C. Liu, H. Guo, S. Zhang, F. Sassa, and K. Hayashi, "A fully inkjet-printed disposable gas sensor matrix with molecularly imprinted gas-selective materials," *npj Flexible Electronics*, vol. 6, no. 1, p. 40, 2022.

[34] O. Ogbeide, G. Bae, W. Yu, E. Morrin, Y. Song, W. Song, Y. Li, B.-L. Su, K.-S. An, and T. Hasan, "Inkjet-printed rgo/binary metal oxide sensor for predictive gas sensing in a mixed environment," *Advanced Functional Materials*, vol. 32, no. 25, p. 2113348, 2022.

[35] B. Andò, S. Baglio, S. Castorina, S. Graziani, M. G. B. Reddy, S. Petralia, M. A. Messina, L. Maugeri, G. Neri, and A. Ferlazzo, "Investigation on a inkjet printed sensor for ammonia detection in liquid media," in *2022 IEEE International Workshop on Metrology for Industry 4.0 & IoT (MetroInd4. 0&IoT)*. IEEE, 2022, pp. 256–260.

[36] S. Khan, S. Ali, A. Khan, and A. Bermak, "Developing pressure sensors from impregnated textile sandwiched in inkjet-printed electrodes," *Journal of Materials Science: Materials in Electronics*, pp. 1–13, 2022.

[37] M. Ma, R. Sun, S. Li, H. Kang, S. Wang, F. Chu, and J. Sun, "Fabricating of double layered flexible pressure sensor with a high-sensitivity based on inkjet printed micro-concave structure," *Sensors and Actuators A: Physical*, vol. 351, p. 114161, 2023.

[38] S. Choi, S. Lee, B. Lee, J. Yoon, C.-y. Lee, T. Kim, and Y. Hong, "Crack-inducing strain sensor array using inkjet-printed silver thin film for underplate and off-centered force sensing applications," *ACS Applied Materials & Interfaces*, vol. 15, no. 3, pp. 4487–4494, 2023.

[39] A. Khan, S. Ali, A. S. Nittala, K. Riaz, and A. Bermak, "Fully inkjet-printed soft wearable strain sensors based on metal/polymer composite sensing films," in *2023 IEEE International Conference on Flexible and Printable Sensors and Systems (FLEPS)*, 2023, pp. 1–4.

[40] S. Sulaiman, A. S. A. Aziz, L. Q. Jun, S. M. H. S. M. Jaafar *et al.*, "Inkjet-printed graphene-based flexible humidity sensor for environmental applications," in *2020 IEEE International Conference on Semiconductor Electronics (ICSE)*. IEEE, 2020, pp. 148–151.

[41] N. Li, Y. Jiang, Y. Xiao, B. Meng, C. Xing, H. Zhang, and Z. Peng, "A fully inkjet-printed transparent humidity sensor based on a ti 3 c 2/ag hybrid for touchless sensing of finger motion," *Nanoscale*, vol. 11, no. 44, pp. 21 522–21 531, 2019.

[42] L. Grob, P. Rinklin, S. Zips, D. Mayer, S. Weidlich, K. Terkan, L. J. Weiß, N. Adly, A. Offenhäusser, and B. Wolfrum, "Inkjet-printed and electroplated 3d electrodes for recording extracellular signals in cell culture," *Sensors*, vol. 21, no. 12, p. 3981, 2021.

[43] N. Adly, S. Weidlich, S. Seyock, F. Brings, A. Yakushenko, A. Offenhäusser, and B. Wolfrum, "Printed microelectrode arrays on soft materials: from pdms to hydrogels," *npj flexible electronics*, vol. 2, no. 1, p. 15, 2018.

[44] G. Gugliandolo, G. Vermiglio, G. Cutroneo, G. Campobello, G. Crupi, and N. Donato, "Development, characterization, and circuit modeling of inkjet-printed coupled ring resonators for application in biological samples," *IEEE Transactions on Instrumentation and Measurement*, vol. 72, pp. 1–10, 2023.

[45] I. Ibanez-Labiano, S. Nourinovin, and A. Alomainy, "Graphene inkjet-printed ultrawideband tapered coplanar-waveguide antenna on kapton substrate," in *2021 15th European Conference on Antennas and Propagation (EuCAP)*, 2021, pp. 1–4.

[46] Z. Liu, Y. Su, and K. Varahramyan, "Inkjet-printed silver conductors using silver nitrate ink and their electrical contacts with conducting polymers," *Thin Solid Films*, vol. 478, no. 1-2, pp. 275–279, 2005.

[47] L. Nayak, S. Mohanty, S. K. Nayak, and A. Ramadoss, "A review on inkjet printing of nanoparticle inks for flexible electronics," *Journal of Materials Chemistry C*, vol. 7, no. 29, pp. 8771–8795, 2019.

[48] J. Song, L. Wang, A. Zibart, and C. Koch, "Corrosion protection of electrically conductive surfaces," *Metals*, vol. 2, no. 4, pp. 450–477, 2012.

[49] R. Salomoni, P. Léo, A. Montemor, B. Rinaldi, and M. Rodrigues, "Antibacterial effect of silver nanoparticles in pseudomonas aeruginosa," *Nanotechnology, science and applications*, pp. 115–121, 2017.

[50] K. Rajan, I. Roppolo, A. Chiappone, S. Bocchini, D. Perrone, and A. Chiolerio, "Silver nanoparticle ink technology: state of the art," *Nanotechnology, science and applications*, pp. 1–13, 2016.

[51] T. Öhlund, A. K. Schuppert, M. Hummelgard, J. Bäckström, H.-E. Nilsson, and H. Olin, "Inkjet fabrication of copper patterns for flexible electronics: using paper with active precoatings," *ACS applied materials & interfaces*, vol. 7, no. 33, pp. 18 273–18 282, 2015.

[52] Y.-T. Kwon, Y.-S. Kim, Y. Lee, S. Kwon, M. Lim, Y. Song, Y.-H. Choa, and W.-H. Yeo, "Ultrahigh conductivity and superior interfacial adhesion of a nanostructured, photonic-sintered copper membrane for printed flexible hybrid electronics," *ACS applied materials & interfaces*, vol. 10, no. 50, pp. 44 071–44 079, 2018.

[53] N. Hayati-Roodbari, A. Wheeldon, C. Hendler, A. Fian, and R. Trattnig, "Ohmic contact formation for inkjet-printed nanoparticle copper inks on highly doped gaas," *Nanotechnology*, vol. 32, no. 22, p. 225205, 2021.

[54] G. Cummins and M. P. Desmulliez, "Inkjet printing of conductive materials: a review," *Circuit world*, vol. 38, no. 4, pp. 193–213, 2012.

[55] K. Rajan, I. Roppolo, A. Chiappone, S. Bocchini, D. Perrone, and A. Chiolerio, "Silver nanoparticle ink technology: state of the art," *Nanotechnology, science and applications*, pp. 1–13, 2016.

[56] R. Garg, *Microstrip antenna design handbook*. Artech house, 2001.

[57] H. R. Khaleel, "Design and fabrication of compact inkjet printed antennas for integration within flexible and wearable electronics," *IEEE Transactions on Components, Packaging and Manufacturing Technology*, vol. 4, no. 10, pp. 1722–1728, 2014.

[58] F. Wang and T. Arslan, "Inkjet-printed antenna on flexible substrate for wearable microwave imaging applications," in *2016 Loughborough Antennas & Propagation Conference (LAPC)*, 2016, pp. 1–4.

[59] J. Zhang, R. Song, X. Zhao, R. Fang, B. Zhang, W. Qian, J. Zhang, C. Liu, and D. He, "Flexible graphene-assembled film-based antenna for wireless wearable sensor with miniaturized size and high sensitivity," *ACS omega*, vol. 5, no. 22, pp. 12 937–12 943, 2020.

[60] M. G. Mayani, F. J. Herraiz-Martínez, J. M. Domingo, R. Giannetti, and C. R.-M. García, "A novel dielectric resonator-based passive sensor for drop-volume binary mixtures classification," *IEEE Sensors Journal*, vol. 21, no. 18, pp. 20 156–20 164, 2021.

[61] G. Guarin, M. Hofmann, J. Nehring, R. Weigel, G. Fischer, and D. Kissinger, "Miniature microwave biosensors: Noninvasive applications," *IEEE Microwave Magazine*, vol. 16, no. 4, pp. 71–86, 2015.

[62] A. Ebrahimi, J. Scott, and K. Ghorbani, "Ultrahigh-sensitivity microwave sensor for microfluidic complex permittivity measurement," *IEEE Transactions on Microwave Theory and Techniques*, vol. 67, no. 10, pp. 4269–4277, 2019.

[63] Q. Xue, X. Tang, Y. Li, H. Liu, and X. Duan, "Contactless and simultaneous measurement of water and acid contaminations in oil using a flexible microstrip sensor," *ACS sensors*, vol. 5, no. 1, pp. 171–179, 2019.

[64] D. M. John, S. Vincent, S. Pathan, P. Kumar, and T. Ali, "Flexible antennas for a sub-6 ghz 5g band: a comprehensive review," *Sensors*, vol. 22, no. 19, p. 7615, 2022.

[65] Z. Duan, S. Shen, and G. Wen, "A compact tri-band filtering antenna system for 5g sub-6 ghz applications," *IEEE Transactions on Antennas and Propagation*, vol. 70, no. 11, pp. 11 097–11 102, 2022.

[66] C.-Y.-D. Sim, H.-Y. Liu, and C.-J. Huang, "Wideband mimo antenna array design for future mobile devices operating in the 5g nr frequency bands n77/n78/n79 and lte band 46," *IEEE Antennas and Wireless Propagation Letters*, vol. 19, no. 1, pp. 74–78, 2020.

[67] P. Turner, B. Garcia, V. Yantchev, G. Dyer, S. Yandrapalli, L. Villanueva, R. Hammond, and V. Plessky, "5 ghz band n79 wideband microacoustic filter using thin lithium niobate membrane," *Electronics letters*, vol. 55, no. 17, pp. 942–944, 2019.

[68] H. Ali, X.-C. Ren, I. Bari, M. A. Bashir, A. M. Hashmi, M. A. Khan, S. I. Majid, N. Jan, W. U. K. Tareen, and M. R. Anjum, "Four-port mimo antenna system for 5g n79 band rf devices," *Electronics*, vol. 11, no. 1, p. 35, 2021.

[69] T. Alam, M. Cheffena, and E. Rajo-Iglesias, "Dual-functional communication and sensing antenna system," *Scientific Reports*, vol. 12, no. 1, p. 20387, 2022.

[70] A. Soltan, R. Sadeghzadeh, and S. Mohammad-Ali-Nezhad, "Microwave sensor for liquid classification and permittivity estimation of dielectric materials," *Sensors and Actuators A: Physical*, vol. 336, p. 113397, 2022.

[71] E. Silavwe, N. Somjit, and I. D. Robertson, "A microfluidic-integrated siw lab-on-substrate sensor for microliter liquid characterization," *IEEE Sensors Journal*, vol. 16, no. 21, pp. 7628–7635, 2016.

[72] A. Kumar, M. S. Rajawat, S. K. Mahto, and R. Sinha, "Metamaterial-inspired complementary split ring resonator sensor and second-order approximation for dielectric characterization of fluid," *Journal of Electronic Materials*, vol. 50, no. 10, pp. 5925–5932, 2021.

[73] E. L. Chuma, Y. Iano, G. Fontgalland, and L. L. Bravo Roger, "Microwave sensor for liquid dielectric characterization based on metamaterial complementary split ring resonator," *IEEE Sensors Journal*, vol. 18, no. 24, pp. 9978–9983, 2018.

[74] E. L. Chuma, Y. Iano, G. Fontgalland, L. L. B. Roger, and H. Loschi, "Pcb-integrated non-destructive microwave sensor for liquid dielectric spectroscopy based on planar metamaterial resonator," *Sensors and Actuators A: Physical*, vol. 312, p. 112112, 2020.

[75] W. Withayachumnankul, A. Tuantranont, C. Fumeaux, and D. Abbott, "Metamaterial-based microfluidic sensor for dielectric characterization," *Sensors and Actuators A: Physical*, vol. 189, pp. 233–237, 2013.

[76] L. Zhu, M. Farhat, Y.-C. Chen, K. N. Salama, and P.-Y. Chen, "A compact, passive frequency-hopping harmonic sensor based on a microfluidic reconfigurable dual-band antenna," *IEEE Sensors Journal*, vol. 20, no. 21, pp. 12 495–12 503, 2020.

[77] L. H. Dai, H. Z. Zhao, X. Zhao, and Y. J. Zhou, "Flexible and printed microwave plasmonic sensor for noninvasive measurement," *IEEE Access*, vol. 8, pp. 163 238–163 243, 2020.

[78] S. G. Kirtania, A. W. Elger, M. R. Hasan, A. Wisniewska, K. Sekhar, T. Karacolak, and P. K. Sekhar, "Flexible antennas: a review," *Micromachines*, vol. 11, no. 9, p. 847, 2020.

[79] O. M. Sanusi, F. A. Ghaffar, A. Shamim, M. Vaseem, Y. Wang, and L. Roy, "Development of a 2.45 ghz antenna for flexible compact radiation dosimeter tags," *IEEE Transactions on Antennas and Propagation*, vol. 67, no. 8, pp. 5063–5072, 2019.

[80] I. I. Labiano and A. Alomainy, "Flexible inkjet-printed graphene antenna on kapton," *Flexible and Printed Electronics*, vol. 6, no. 2, p. 025010, 2021.

[81] Y. Dong, H. Toyao, and T. Itoh, "Design and characterization of miniaturized patch antennas loaded with complementary split-ring resonators," *IEEE Transactions on Antennas and Propagation*, vol. 60, no. 2, pp. 772–785, 2012.

[82] W.-Y. Park and S. Lim, "Miniaturized substrate integrated waveguide (siw) bandpass filter loaded with double-sided-complementary split ring resonators (ds-csrrs)," in *2011 41st European Microwave Conference*, 2011, pp. 740–743.

[83] NovaCentrix. (2022) Js-a291 silver nanoparticle ink. [Online]. Available: https://www.novacentrix.com/product/js-a291-silver-nanoparticles/

[84] S. Wünscher, R. Abbel, J. Perelaer, and U. S. Schubert, "Progress of alternative sintering approaches of inkjet-printed metal inks and their application for manufacturing of flexible electronic devices," *Journal of Materials Chemistry C*, vol. 2, no. 48, pp. 10 232–10 261, 2014.

[85] S. Jang, Y. Seo, J. Choi, T. Kim, J. Cho, S. Kim, and D. Kim, "Sintering of inkjet printed copper nanoparticles for flexible electronics," *Scripta Materialia*, vol. 62, no. 5, pp. 258–261, 2010.

[86] D. Kim and J. Moon, "Highly conductive ink jet printed films of nanosilver particles for printable electronics," *Electrochemical and Solid-State Letters*, vol. 8, no. 11, p. J30, 2005.

[87] Y. Khan, F. J. Pavinatto, M. C. Lin, A. Liao, S. L. Swisher, K. Mann, V. Subramanian, M. M. Maharbiz, and A. C. Arias, "Inkjet-printed flexible gold electrode arrays for bioelectronic interfaces," *Advanced Functional Materials*, vol. 26, no. 7, pp. 1004–1013, 2016.

[88] M. Rebato, J. Park, P. Popovski, E. De Carvalho, and M. Zorzi, "Stochastic geometric coverage analysis in mmwave cellular networks with realistic channel and antenna radiation models," *IEEE Transactions on Communications*, vol. 67, no. 5, pp. 3736–3752, 2019.

[89] M. Zada and H. Yoo, "Miniaturized dual band antennas for intra-oral tongue drive system in the ism bands 433 mhz and 915 mhz: Design, safety, and link budget considerations," *IEEE transactions on antennas and propagation*, vol. 67, no. 9, pp. 5843–5852, 2019.

[90] D. R. Jackson, "Introduction to microstrip antennas," in *Proc. IEEE Int. Symp. Antennas Propag. USNC URSI Nat. Radio Sci. Meeting*, 2013, pp. 1–179.

[91] D. Nascimento, R. Schildberg, and J. d. S. Lacava, "New considerations in the design of low-cost probe-fed truncated corner microstrip antennas for gps applications," in *2007 IEEE Antennas and Propagation Society International Symposium*. IEEE, 2007, pp. 749–752.

[92] L. Zhu, N. Alsaab, M. M.-C. Cheng, and P.-Y. Chen, "A zero-power ubiquitous wireless liquid-level sensor based on microfluidic-integrated microstrip antenna," *IEEE Journal of Radio Frequency Identification*, vol. 4, no. 3, pp. 265–274, 2020.

[93] K. Zhang, P. J. Soh, and S. Yan, "Meta-wearable antennas—a review of metamaterial based antennas in wireless body area networks," *Materials*, vol. 14, no. 1, p. 149, 2020.

[94] P. K. Sharma and N. Gupta, "A cpw-fed circular srr-inspired flexible antenna using polydimethylsiloxane (pdms) substrate for wlan and wban applications," *IEEE Journal on Flexible Electronics*, vol. 1, no. 1, pp. 39–46, 2022.

[95] K. Sreelakshmi, G. S. Rao, and M. N. V. S. S. Kumar, "A compact grounded asymmetric coplanar strip-fed flexible multiband reconfigurable antenna for wireless applications," *IEEE Access*, vol. 8, pp. 194 497–194 507, 2020.

[96] A. S. M. Sayem, A. Lalbakhsh, K. P. Esselle, J. L. Buckley, B. O'Flynn, and R. B. V. B. Simorangkir, "Flexible transparent antennas: Advancements, challenges, and prospects," *IEEE Open Journal of Antennas and Propagation*, vol. 3, pp. 1109–1133, 2022.

[97] H. A. Elmobarak, M. Himdi, X. Castel, S. K. A. Rahim, and T. K. Geok, "Flexible patch antenna array operating at microwaves based on thin composite material," *IEEE Access*, vol. 10, pp. 115 663–115 672, 2022.

[98] A. S. M. Alqadami, A. E. Stancombe, K. S. Bialkowski, and A. Abbosh, "Flexible meander-line antenna array for wearable electromagnetic head imaging," *IEEE Transactions on Antennas and Propagation*, vol. 69, no. 7, pp. 4206–4211, 2021.

[99] 3A Composites Core Materials company. (2023) AIREX® T10.100 PET foam. [Online]. Available: https://www.3accorematerials.com/en/markets-and-products/airex-foam/airex-t10-pet-foam/

[100] H. Li, J. Du, X.-X. Yang, and S. Gao, "Low-profile all-textile multiband microstrip circular patch antenna for wban applications," *IEEE Antennas and Wireless Propagation Letters*, vol. 21, no. 4, pp. 779–783, 2022.

[101] Y. Wang, M.-C. Tang, S. Chen, L. Li, D. Li, K.-Z. Hu, and M. Li, "Design of low-cost, flexible, uniplanar, electrically small, quasi-isotropic antenna," *IEEE Antennas and Wireless Propagation Letters*, vol. 18, no. 8, pp. 1646–1650, 2019.

[102] H. Qiu, H. Liu, X. Jia, Z.-Y. Jiang, Y.-H. Liu, J. Xu, T. Lu, M. Shao, T.-L. Ren, and K. J. Chen, "Compact, flexible, and transparent antennas based on embedded metallic mesh for wearable devices in 5g wireless network," *IEEE Transactions on Antennas and Propagation*, vol. 69, no. 4, pp. 1864–1873, 2020.

[103] A. van Bezooijen, M. A. de Jongh, F. van Straten, R. Mahmoudi, and A. H. M. van Roermund, "Adaptive impedance-matching techniques for controlling l networks," *IEEE Transactions on Circuits and Systems I: Regular Papers*, vol. 57, no. 2, pp. 495–505, 2010.

[104] F. Chan Wai Po, E. de Foucauld, D. Morche, P. Vincent, and E. Kerherve, "A novel method for synthesizing an automatic matching network and its control unit," *IEEE Transactions on Circuits and Systems I: Regular Papers*, vol. 58, no. 9, pp. 2225–2236, 2011.

[105] M. Alibakhshikenari, B. S. Virdee, P. Shukla, C. H. See, R. A. Abd-Alhameed, F. Falcone, and E. Limiti, "Improved adaptive impedance matching for rf front-end systems of wireless transceivers," *Scientific Reports*, vol. 10, no. 1, pp. 1–11, 2020.

[106] M. Alibakhshikenari, B. S. Virdee, L. Azpilicueta, C. H. See, R. Abd-Alhameed, A. A. Althuwayb, F. Falcone, I. Huynen, T. A. Denidni, and E. Limiti, "Optimum power transfer in rf front end systems using adaptive impedance matching technique," *Scientific Reports*, vol. 11, no. 1, p. 11825, 2021.

[107] K. Alp, F. Bagci, and B. Akaoglu, "A metamaterial-based dielectric sensor for characterization of ethanol/1-pentanol binary liquid mixtures at dual bands," *Applied Physics A*, vol. 129, no. 8, p. 556, 2023.

[108] A. Karatepe, O. Akgöl, Y. I. Abdulkarim, Ş. Dalgac, F. F. Muhammadsharif, H. N. Awl, L. Deng, E. Ünal, M. Karaaslan, L. Heng *et al.*, "Multipurpose chemical liquid sensing applications by microwave approach," *PloS one*, vol. 15, no. 5, p. e0232460, 2020.

[109] Sigma-Aldrich®. (2023) Snap cap vials. [Online]. Available: https://www.sigmaaldrich.com/NO/en/product/aldrich/baf175750003

[110] A. Sihvola, "Mixing rules with complex dielectric coefficients," *Subsurface sensing technologies and applications*, vol. 1, no. 4, pp. 393–415, 2000.

[111] A. A. Helmy, S. Kabiri, M. M. Bajestan, and K. Entesari, "Complex permittivity detection of organic chemicals and mixtures using a 0.5–3-ghz miniaturized spectroscopy system," *IEEE Transactions on Microwave Theory and Techniques*, vol. 61, no. 12, pp. 4646–4659, 2013.

[112] M. Mohsen-Nia, H. Amiri, and B. Jazi, "Dielectric constants of water, methanol, ethanol, butanol and acetone: measurement and computational study," *Journal of Solution Chemistry*, vol. 39, pp. 701–708, 2010.

[113] A. Gregory and R. Clarke, "Traceable measurements of the static permittivity of dielectric reference liquids over the temperature range 5–50 c," *Measurement Science and Technology*, vol. 16, no. 7, p. 1506, 2005.

[114] L. Zhu, N. Alsaab, M. M.-C. Cheng, and P.-Y. Chen, "A zero-power ubiquitous wireless liquid-level sensor based on microfluidic-integrated microstrip antenna," *IEEE Journal of Radio Frequency Identification*, vol. 4, no. 3, pp. 265–274, 2020.

[115] X. Han, X. Li, Y. Zhou, Z. Ma, P. Peng, C. Fu, and L. Qiao, "Microwave sensor loaded with complementary curved ring resonator for material permittivity detection," *IEEE Sensors Journal*, vol. 22, no. 21, pp. 20 456–20 463, 2022.

[116] M. Palandoken, C. Gocen, T. Khan, Z. Zakaria, I. Elfergani, C. Zebiri, J. Rodriguez, and R. A. Abd-Alhameed, "Novel microwave fluid sensor for complex dielectric parameter measurement of ethanol–water solution," *IEEE Sensors Journal*, vol. 23, no. 13, pp. 14 074–14 083, 2023.

[117] S. Kumar, R. Singh, Q. Yang, S. Cheng, B. Zhang, and B. K. Kaushik, "Highly sensitive, selective and portable sensor probe using germanium-doped photosensitive optical fiber for ascorbic acid detection," *IEEE Sensors Journal*, vol. 21, no. 1, pp. 62–70, 2020.

[118] B. K. Kaushik, L. Singh, R. Singh, G. Zhu, B. Zhang, Q. Wang, and S. Kumar, "Detection of collagen-iv using highly reflective metal nanoparticles—immobilized photosensitive optical fiber-based mzi structure," *IEEE Transactions on NanoBioscience*, vol. 19, no. 3, pp. 477–484, 2020.

[119] B. Kaur, S. Kumar, and B. K. Kaushik, "2d materials-based fiber optic spr biosensor for cancer detection at 1550 nm," *IEEE Sensors Journal*, vol. 21, no. 21, pp. 23 957–23 964, 2021.

[120] V. S. Chaudhary, D. Kumar, B. P. Pandey, and S. Kumar, "Advances in photonic crystal fiber-based sensor for detection of physical and biochemical parameters-a review," *IEEE Sensors Journal*, 2022.

Kabir Hossain (Graduate Student Member, IEEE) received the B.Eng. (Hons.) in Communication Engineering and M.Sc. in Communication Engineering (by research) degrees from Universiti Malaysia Perlis (UniMAP), Malaysia, in 2019 and 2021, respectively. He is currently pursuing his Ph.D. degree under the supervision of Prof. Cheffena at the Norwegian University of Science and Technology (NTNU), Norway. His broad area of interests include, but not limited to antennas and related technologies; with specific interest in their applications in wearables/body area communication; antenna sensors, reconfigurable antennas; EM metamaterial; metasurfaces; massive MIMO, microwave imaging; and wireless techniques for healthcare and B5G/6G. He received the Best Paper Award sponsored by IEEE APS-MTT chapter of Scotland at 5th International Conference on the UK-China Emerging Technologies (UCET 2020), Glasgow, UK. He also received the Best Paper Award at the 1st International Conference on Engineering and Technology (ICoEngTech) 2021, Perlis, Malaysia.

Yu Dang (Graduate Student Member, IEEE) received the B.S. degree in microwave technology and the M.S. degree in microwave technology from the Harbin Institute of Technology, in 2017 and 2019, respectively. He is currently pursuing his PhD degree under the supervision of Prof. Cheffena at the Norwegian University of Science and Technology (NTNU), Norway. His research interests include antenna sensor, metasurface-based imaging, and MIMO antenna.

Michael Cheffena received the M.Sc. degree in electronics and computer technology from the University of Oslo, Oslo, Norway, in 2005, and the Ph.D. degree from the Norwegian University of Science and Technology (NTNU), Trondheim, Norway, in 2008

In 2007, he was a Visiting Researcher at the Communications Research Center, Ottawa, ON, Canada. From 2009 to 2010, he conducted a postdoctoral study at the University Graduate Center, Kjeller, Norway, and the French Space Agency, Toulouse, France. He is currently a Full Professor at NTNU, Gjøvik, Norway. His research interests include the modeling and prediction of propagation radio channels, signal processing, medium access control protocol design, antenna sensors, and sensor systems.